ADVANCED FUNCTIONAL MATERIALS
www.afm-journal.de

3D Transformable Modular Kirigami Based Programmable Metamaterials

*Yanbin Li, Qiuting Zhang, Yaoye Hong, and Jie Yin**

Kirigami, the ancient paper art of cutting, has recently emerged as a new approach to construct metamaterials with novel properties imparted by cuts. However, most studies are limited to thin sheets-based 2D kirigami metamaterials with specific forms and limited reconfigurability due to planar connection constraints of cut units. Here, 3D modular kirigami is introduced by cutting bulk materials into spatially closed-loop connected cut cubes to construct a new class of 3D kirigami metamaterials. The module is transformable with multiple degrees of freedom that can transform into versatile distinct daughter building blocks. Their conformable assembly creates a wealth of reconfigurable and disassemblable metamaterials with diverse structures and unique properties, including reconfigurable 1D column-like materials, 2D lattice-like metamaterials with phase transition of chirality, as well as 3D frustration-free multilayered metamaterials with 3D auxetic behaviors and programmable deformation modes. This study largely expands the design space of kirigami metamaterials from 2D to 3D.

1. Introduction

Mechanical metamaterials are artificial materials constructed through rational design of architectural structures and spatial arrangement of 2D and 3D building blocks[1–5] to achieve unprecedented physical properties, such as ultra-stiffness,[6] auxeticity,[7] negative thermal expansion,[8–10] and negative compressibility.[11,12] Recently, kirigami, the ancient paper art of cutting, has emerged as a new way to construct mechanical metamaterials by utilizing the uniqueness of cuts. Starting from 2D thin sheets of materials, different cutting patterns impart 2D kirigami metamaterials with new properties such as tunable negative Poisson's ratios,[13–15] large stretchability,[16–22] multistabilities,[23] giant negative thermal expansion,[24] and programmable and tunable mechanical properties.[25–27] However, beyond 2D thin sheets, it remains largely unexplored concerning how to extend cutting to 3D bulk materials (i.e., 3D spatial cutting) for constructing 3D kirigami metamaterials.[28–30] Spatial cutting could release the constrained degrees of freedom (DOF) in 2D kirigami metamaterials to allow transformation in distinct 2D and 3D deformation modes, thus largely expanding the design space of kirigami metamaterials. In principle, the design of 3D metamaterials can be considered as a spatial filling tessellation problem. Periodic metamaterials favor cooperative structural deformation from their geometrically compatible periodic units,[3,31] while in nonperiodic metamaterials, intrinsic incompatible geometric frustrations often occur after deformation,[32] which should be avoided. Thus, the challenge of constructing 3D periodic/non-periodic kirigami metamaterials resides in the rational design of 3D kirigami modules as building blocks and their tessellation to ensure deformation compatibility without geometric frustrations.

Here, we propose a 3D transformable modular kirigami strategy to create a new class of frustration-free, reconfigurable, and re-assemblable kirigami metamaterials with a programmable mechanical response. Unlike thin sheet-based conventional 2D kirigami metamaterials,[13–26] we start with cutting bulk materials into spatially closed-loop hinged 3D cubes to generate a 3D modular kirigami with multiple DOF (**Figure 1**a), which could further evolve into over 0.3 million derived modules. The 3D modular kirigami can transform in 3Ds into versatile daughter modules in distinct configurations (Figure 1b). The complementary topological features between transformed 3D kirigami modules not only enable assembly into reconfigurable modular architectures without the need for bonding connections, but also facilitate disassembly for reuse and re-assembly for new structures. By utilizing combinatorial arrangements of compatible and conformable modules via stacking and tessellation, we build a library of disassemblable multidimensional kirigami metamaterials with unique deformation independence and programmable deformation modes. This research paves a new way to design a wealth of both periodic and quasiperiodic metamaterials with unprecedented material properties adaptive to diverse applications through combinatorial modular assembly and disassembly.

Y. Li, Y. Hong, J. Yin
Department of Mechanical and Aerospace Engineering
North Carolina State University
Raleigh, NC 27695, USA
E-mail: jyin8@ncsu.edu
Q. Zhang
Department of Molecular
Cellular and Developmental Biology
Yale University
New Haven, CT 06520, USA

The ORCID identification number(s) for the author(s) of this article can be found under https://doi.org/10.1002/adfm.202105641.

DOI: 10.1002/adfm.202105641

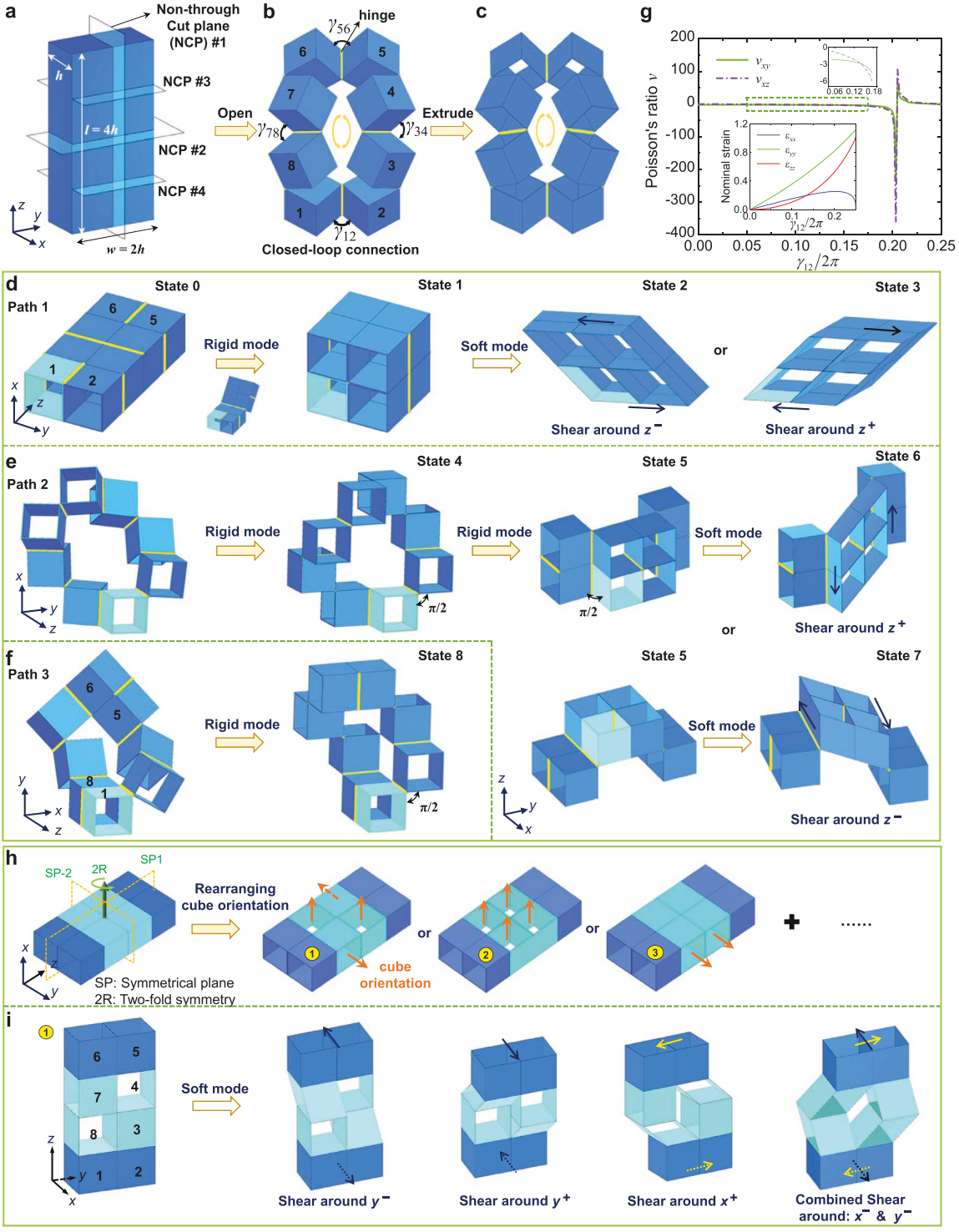

Figure 1. 3D transformable modular kirigami via both rigid and soft modes. a–c) Schematic construction of a 3D modular kirigami. In (a), a solid cuboid is first dissected by four non-through cutting planes into eight identical cubes connected through elastic torsional hinges (highlighted in yellow lines) to allow reconfigure in 3D by rigid rotation mode (b), followed by extruding to generate connected thin-walled cubes (c), allowing deforming extruded cubes through the soft mode of thin wall shearing. γ_{ij} is the dihedral angle between two adjacent cubes *i* and *j*. d–f) Its eight representative transformed configuration states through three different transition paths via both solid mode and soft mode. In (d), path 1 without opening cuts; in (e), path 2 with all cuts open; in (f), path 3 with two pairs of cubes (cube 5 and 6, cube 8 and 1) being bonded in path 2. g) profile of Poisson's ratio ν_{xy} and ν_{xz} versus opening angle $0 \leq \gamma_{12}/2 \leq \pi/2$ during transition path 2 in (e). Top inset: zoomed view of Poisson's ratio versus $\gamma_{12}/2$ profile. Bottom inset: profile of nominal strains along three axial directions versus $\gamma_{12}/2$. h) Examples of three derived 3D basic modules by rearranging the orientations of the middle four cubes. i) Multiple reconfigured structural forms through soft shearing mode around *x* and *y* axis in the derived 3D module of example ① in (h).

2. Results

2.1. Transformable 3D Modular Kirigami and Their Derivatives

Figure 1a–c illustrates the design of a transformable 3D modular kirigami by following two procedures. First, starting from a solid 3D cuboid with length l, width w, and height h ($l = 2w = 4h$), we introduce four non-through cut planes (i.e., spatial cuts rather than line cuts or slits in 2D kirigami sheets) to dissect the cuboid into eight discretely connected identical cubes with size h through eight elastic torsional hinges (Figure 1a). Each cube is connected with two neighboring cubes through two orthogonal line hinges to form a spatial closed-loop connection, allowing rigid rotation of cubes around the hinges to transform out of plane to open all the cuts (Figure 1b), that is, a rigid mode. Such a spatial line hinge connection largely frees the constrained in-plane and out-of-plane rotations of rigid cut plates in conventional thin sheet-based 2D kirigami metamaterials,[13–26] as well as the constrained 3D rotations of origami-inspired, extruded cube unit cell without cuts.[33]

When surface contact is allowed during transformation, the 3D modular kirigami exhibits 2 zero-energy modes by assuming free rotational hinges (see Section S1, Supporting Information), resulting in a multi-DOF structure with its number of DOF N_{DOFs} being $N_{\mathrm{DOFs}} = 1$ or 2 depending on its transformed configuration.

Second, further extruded cut along the z-axis generates connected thin-walled cubes with uniform orientations that are defined by the extruded direction (Figure 1c). When considering thin-walled cubes composed of four rigid plates connected through internal elastic torsional hinges, it enables an additional soft mode by shearing the cube through rotating the rigid walls around the internal hinges (Figure 1d,e).

When setting the dihedral angle $\gamma_{ij} = k\pi / 2$ ($k = 0, 1, 2$) of adjacent cubes i and j numbered counterclockwise in Figure 1b, Figure 1d–f show that starting from its original State 0, it can fold and reconfigure into three representative daughter building blocks (State 1, 4, and 8) in eight different configuration states through both rigid mode and soft mode by following three reconfiguration paths (Video S1, Supporting Information). In reconfiguration path 1 (Figure 1d), it transforms to a cubic shape (State 1, $1 \le N_{\mathrm{DOFs}} \le 2$) through rigid mode by rotating the dihedral angles of $\gamma_{34} = \gamma_{78}$ from 0 to π. It can be further sheared around negative z-axis (z^-, State 2) or positive z-axis (z^+, State 3) through soft mode. In reconfiguration path 2 (Figure 1e and Figure S1a, Supporting Information), all the cuts are open and settled with $\gamma_{ij} = \pi / 2$ to form a symmetric configuration, generating a pore in the middle (State 4, $N_{\mathrm{DOFs}} = 1$). When the pore is closed, it transits to State 5 ($N_{\mathrm{DOFs}} = 2$) through rigid mode. Similarly, State 5 can be further sheared around z^+ (State 6) and z^- axis (State 7). Reconfiguration path 3 (Figure 1f) is a special case of path 2, where two pairs of neighboring cubes (cube 5 and 6, cube 8 and 1) are constrained without allowing relative rotations. Thus, it becomes an asymmetric structure with a single DOF shown as State 8 ($N_{\mathrm{DOFs}} = 1$) of Figure 1f, which cannot further deform via soft mode.

Interestingly, during the rigid transformation from State 0 to State 4 in reconfiguration path 2, as γ_{12} increases from 0 to $\pi / 2$, both nominal normal strains ε_{yy} and ε_{zz} along respective y and z-axis increase monotonically, while ε_{xx} exhibits a peak (inset of Figure 1g). Consequently, its Poisson's ratios $\nu_{xy} = -\varepsilon_{xx} / \varepsilon_{yy}$ and $\nu_{xz} = -\varepsilon_{xx} / \varepsilon_{zz}$ transit from negative to positive values with a turning jump point at the peak nominal strain ε_{xx} (Figure 1g) caused by the unique structural form (Figure S1, see Section S2, Supporting Information, for more details).

We note that such a 3D kirigami modular design could further evolve into over 31 845 derived basic modules as potential building blocks through combinatorial designs of both different thin-walled cube orientations (Figure 1h) and relocated spatial hinge connections (Figure S2, see Section S3, Supporting Information). Such a combinatorial design could not be achieved in 2D thin sheet-based kirigami metamaterials[13–26] and origami-inspired cube-based transformable unit cells.[33] Figure 1h shows three derived examples by rearranging the orientations of the middle four voxelated cubes (highlighted in light green color) from z-axis in the original module to x-axis (②) or y-axis (③) or combined (①). Consequently, it leads to different reconfigured structures through the soft mode of local shearing in the voxelated cubes. For example, Figure 1i shows a derived module ① with cube 3 and 7's orientation along y-axis while cube 4 and 8's orientation is along x-axis. It can reconfigure into at least 4 different configurations through local shearing around positive or negative y-axis or x-axis or combined (Figure 1i). The combinations of building blocks in terms of voxelated cube orientations and spatial hinge arrangements will provide enormous design space for constructing reconfigurable, re-assemblable, reprogrammable, and multi-dimensional architected metamaterials through modular assembly and disassembly.

2.2. 1D and 2D Modular Metamaterials

Through vertical stacking and in-plane tessellation of derivative transformable building blocks, we can generate reconfigurable 1D column-like and 2D lattice-like (**Figure 2**) periodic architected materials, respectively. We fabricate the 3D modular kirigami prototypes on a centimeter scale made from cardboard through laser cutting (see Experimental Section, Figure S3, Supporting Information).

During modular assembly, two geometrical compatibility conditions need to be satisfied to ensure coherent deformation and structural reconfiguration.[32] First, at shared boundary surfaces, pairs of neighboring blocks should display complementary shapes, such that adjacent blocks can be adapted for a tight fit without protrusions regardless of further deformations. Second, regarding the in-plane alignment and tessellation of blocks, all the blocks should fit with matched complementary topologies to ensure cooperative deformation among all units.

2.2.1. 1D Column-Like Metamaterials

Guided by the above compatible conditions, Figure 2a,b presents two examples of assembled 1D column-like compact materials. One is constructed by directly stacking the single transformed State 4 module (Figure 2a(i)); the other is by

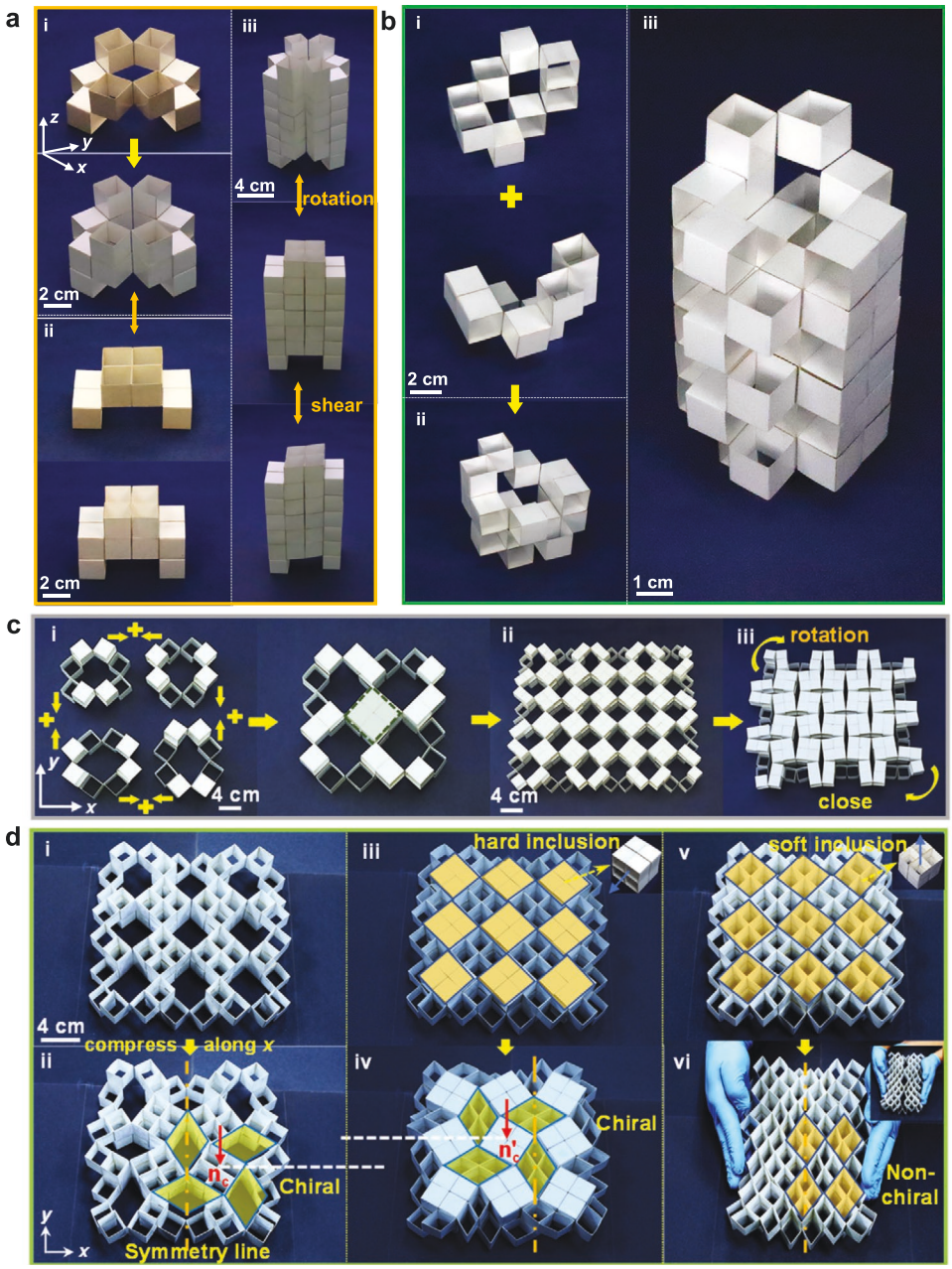

Figure 2. Periodic 1D column-like and 2D lattice-like metamaterials through the conformable modular assembly. a,b) Prototypes of 1D column-like metamaterials by vertically stacking the same building blocks (state 4 in (a) and state 8 in (b)) without bonding. The created 1D metamaterial is reconfigurable with a single DOF through rigid rotation or soft shearing mode to close or open the pores (a), while it is nondeformable in (b) with both deformation modes locked. c) 2D lattice-like metamaterials by in-plane tessellation of transformed modules with complimentary topological configurations. d) Tunable deformation chirality in 2D metamaterials through the same filled inclusions but different cube orientations under uniaxial compression. i,ii) 2D metamaterial as matrix composed of assembled State 4 modules with uniform cube orientation exhibits deformation chirality centering at matrix (n_c) under compression. iii,iv) After filling the matrix with hard inclusions that possess different cube orientations (inset), the deformation chirality center shifts from the matrix to the rigid inclusion (n^-_c). v,vi) It transits to a non-chiral structure after filling the matrix with soft inclusions that possess the same cube orientation (inset of v). The inclusions are highlighted in yellow color in iii and v.

orthogonally stacking the same transformed State 8 module (Figure 2b(i)). They are joined without bonding boundary faces of adjacent units but through complementary shapes between two daughter transformable building blocks, thus, they are disassemblable. The former is reconfigurable and deforms collectively the same as its constituent single module in Figure 2a(i). The void in the center can be closed under lateral compression through rigid mode (transition from State 4 to State 5 in Figure 1e), which can be further sheared through soft mode (transition from State 5 to State 6 in Figure 1e) as shown in Figure 2a(iii). By contrast, the latter shown in Figure 2b(iii) is rigid and non-deformable due to the heterogeneous cube

orientations and surface contacts; however, it can reconfigure in soft shearing mode after setting all cubes with uniform orientations (Figure S4, Supporting Information).

2.2.2. 2D Lattice-Like Metamaterials

Rather than stacking, tessellating building blocks of transformed State 4 of Figure 1e with in-plane complementary shapes along two orthogonal directions (Figure 2c(i)) forms a periodic 2D lattice-like material (Figure 2c(ii)), which satisfies both geometrical compatibility conditions. It takes a similar structural form to the conventional kirigami sheet with square-cut units.[13,20] It shows a constant negative Poisson's ratio of –1 by allowing only the rotation mode of rigidly assembled cubes (highlighted in green color) to close the voids under compression (Figure 2c(iii)).

Furthermore, such voids in the 2D materials matrix provide sites to fill structurally compatible transformed cubic blocks of State 1 as inclusions, thus potentially generating more varieties of assembled 2D architected materials with tunable materials response by selectively filling or removing the porous matrix with inclusions. As one example, in Figure 2d(i), we set the assembled matrix with uniform cube orientations along the thickness direction. Under compression, it shows a chiral deformation centering around the assembled cube (Figure 2d(ii)). We demonstrate that depending on the placement orientation of inserted State 1 module (see inset of Figure 2d(iii–v)), the 2D lattice-like material could exhibit topologically distinct structural phase transitions under compression. When the inclusions are placed with their cube orientations orthogonally to the matrix (Figure 2d(iii)), such inclusions become rigid and are much stiffer than the matrix, thus, upon compression, the hybrid material undergoes soft shearing deformation in the matrix accompanied by the rigid rotation of the inclusions (Figure 2d(iv)). Correspondingly, the chirality center shifts from the matrix in Figure 2d(ii) to the inclusions in Figure 2d(iv). By contrast, when the inclusions are placed with the same cube orientations as the matrix (Figure 2d(v)), the deformation chirality in Figure 2d(ii),(iv) is eliminated as shown in Figure 2d(vi). Consequently, in contrast to the negative Poisson's ratio of –1 in both chiral structures, the non-chiral structure shows a positive Poisson's ratio, where the soft inclusions possess the same stiffness as the matrix and the whole structure deforms under soft shearing modes in both the matrix and inclusions.

2.3. 3D Modular Architected Metamaterials

2.3.1. Construction of Frustration-Free 3D Metamaterials

Next, inspired by the mortise-and-tenon joining method (also known as "Sun Mao") in ancient China as illustrated in **Figure 3**a, a nail-free technique of constructing stable architectures,[34] we utilize the conformable fit between different combinations of 3D modular kirigami to create a new class of quasiperiodic yet frustration-free 3D metamaterial that possesses a long-range order.[35]

As schematically illustrated in Figure 3b, the 3D metamaterial is formed by following two steps through the mortise-and-tenon joining technique without any bonding. First, the tightly fitted square columns that have internal structures as tenons are inserted into the square-shaped voids (i.e., mortise) of the created 2D lattice-like materials in Figure 2c(ii) with a depth of h forming a single stacking layer. Second, stacking and assembling the layers of columns and 2D materials along the z-axis through the mortise-and-tenon joining technique (Figure 3b(ii)) with an inserted depth of h forms a multilayered architected material (see the schematic model in Figure 3b(iii) and physical model in Figure S5, Supporting Information). The square column is composed of two line-hinged base kirigami modules (State 0 of Figure 1d) by connecting the two pairs of side edges of the top and bottom cubes (middle of Figure 3c). The arrays of square voids in the 2D layer play the role of mortises to join the columns in different patterns tightly (Video S2, Supporting Information). The column can be divided into three segments in terms of connection purpose, that is, tenon-connector-tenon. The four cubes on the top and bottom segment highlighted in blue color represent the tenons inserted into the voids of 2D layers, and the eight cubes in the middle segment highlighted in green color represent the column connector with internal structures (middle of Figure 3c).

2.3.2. Combinatorial Multiple Deformation Modes in Square Columns

The potential deformation modes of the proposed 3D metamaterials in a long-range order are determined by both the mortise-and-tenon connectivity and the internal structures of column connectors. Considering the heterogeneously voxelated cubes and conditional hinge positions in the square column, the combinatorial number of evolved structural forms in the column could be over $31\,845^2 \approx 10^9$ (See Section S5.1, Supporting Information). However, we can readily classify them into $2^3 = 8$ deformation motifs in terms of combinational deformability ("+" denotes deformable and "–" denotes rigid and non-deformable) in the three-segmented column from top to bottom, that is, (+, +, +), (+, +, –), (+, –, +), (–, +, +), (+, –, –), (–, +, –), (–, –, +), and (–, –, –). For example, (+, +, +) motif means that all the three segments are deformable via soft mode, and (+, –, +) motif means that both the top and bottom tenons are deformable while the middle connector is non-deformable, see more examples with stretchable and compressible features in Figure S6 and Video S2, Supporting Information.

Figure 3c shows two representative examples of columns with motifs of (+, +, +) (right) and (–, +, –) (left). We note that the square columns with identical structural forms can deform distinctly by manipulating hinge positions. For both columns, the middle connector can deform in multiple modes through the soft mode of internal structures under compression. Both top and bottom tenons are stiff in the (–, +, –) column but are deformable through soft mode in the (+, +, +) column. Notably, for the (+, +, +) column, we find that both top and bottom tenons can be independently twisted without deforming the middle connector.

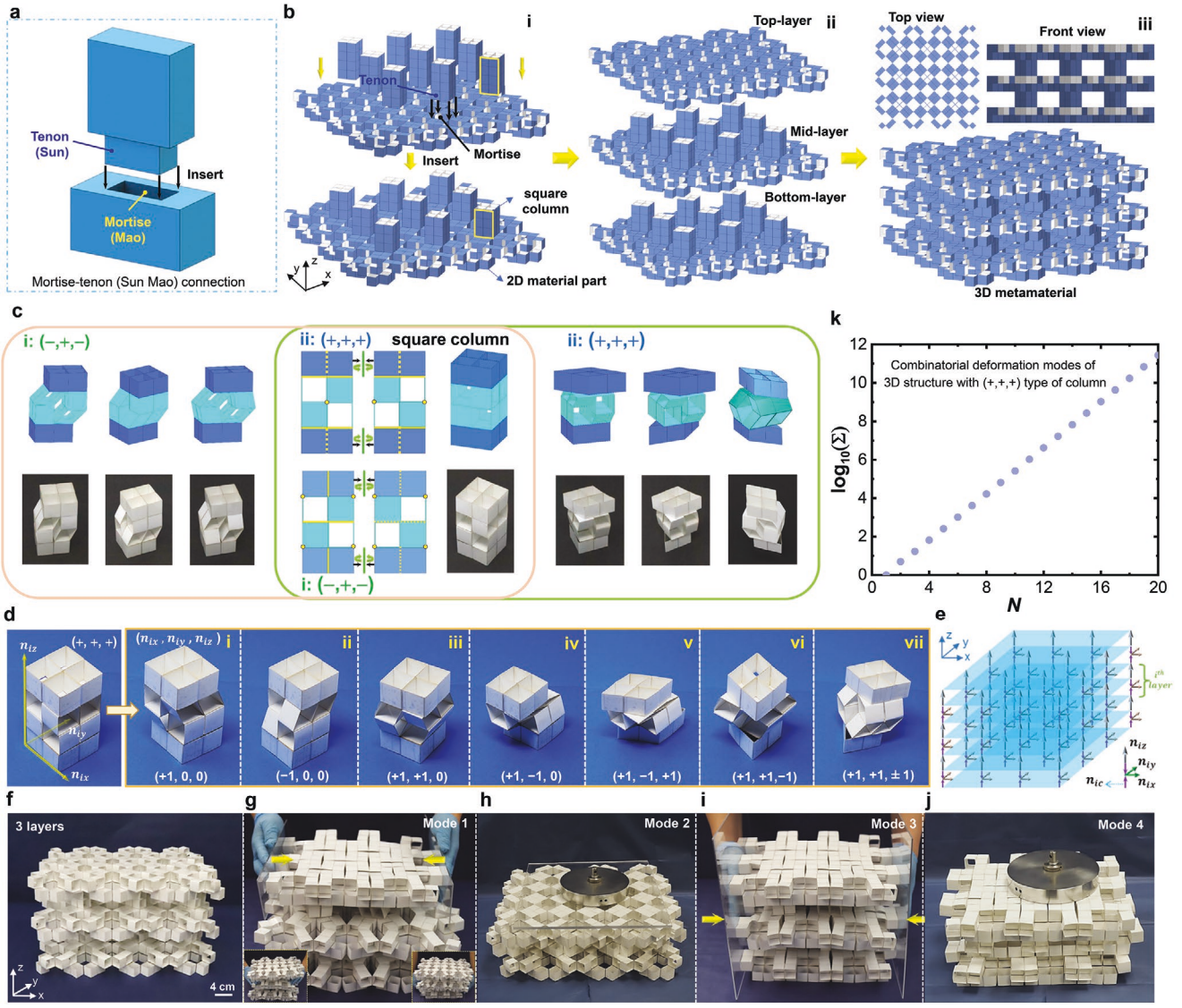

Figure 3. 3D quasiperiodic metamaterial. a) Schematic illustration of the concept of mortise-tenon joining method (also known as "Sunmao") in ancient Chinese architecture utilized in the jointless assembly of 3D architected material. b) Schematic construction of multilayered architected metamaterials via Chinese mortise-and-tenon connection technique by filling the voids (mortises) of 2D assembled material layers (same as Figure 2c(ii)) with inserted arrays of tightly fitted square columns (two ends as tenons). c) Two representative designs of square columns composed of two line-hinged basic kirigami modules (State 0) by manipulating hinge positions (middle). The two columns have identical structural forms but different deformation modes in the top, middle, and bottom segments. Column type 1 (−, +, −) can only deform its middle segment through shearing of the voxelated cubes (left). In column type 2 (+, +, +), all the three segments can deform independently (right). d) Combinatorial deformation modes for column type 2 in (c) characterized by different values of rotation spin (n_{ix}, n_{iy}, n_{iz}). e) Mapping of the assembled 3D architectures to the simplified spin frame, where (n_{ix}, n_{iy}, n_{iz}) are rotation spins along the *x*, *y*, and *z*-axis, respectively. $n_{ic} = n_{iz}$ is the rotation spin in the 2D material layer. f) Prototypes of cardboard-based three-layered metamaterial composed of three layers of 6 × 6 2D materials and two layers of 2 × 3 square columns (the same column arrangement as (a) with spin configuration of (n_{ix}, n_{iy}, n_{iz}) = (±1, ±1, ±1). The composed square column (+, +, +) is the same as (e). g) Demonstration of its local independent deformation mode between each 2D materials layer and square columns layer (Mode 1) in (f). h–j) Demonstration of its global cooperative deformation modes under vertical compression by deforming columns only (Mode 2, (h)), under lateral compression by deforming 2D materials layers only (Mode 3, (i)), under combined vertical and lateral compression by deforming all layers (Mode 4, (j)). k) Total number (Σ) of combinatorial deformation modes for 3D architected materials with the number of *N* layers of 2D material parts bridged with column type (+, +, +).

To further characterize different deformation modes in the *i*th column layer, we use the polarized spins (n_{ix}, n_{iy}, n_{iz}) to represent local directional shearing in voxelated cubes via soft mode along *x*, *y*, and *z*-axis, respectively. Each polarized spin takes values of −1, +1, or 0, where +1 and −1 represent polarized shearing around the positive (x^+, y^+, and z^+) and negative axial direction (x^-, y^-, and z^-) as illustrated in Figure 1i, respectively, while 0 implies non-shearable and thus rigid along that polarized direction. Figure 3d shows that the (+, +, +) column has over 7 deformation modes through combinatorial local shearing, where each mode can be characterized by different spin values of (n_{ix}, n_{iy}, n_{iz}). For example, the deformation mode

in Figure 3d(i) can be characterized by spin values of (n_{ix}, n_{iy}, n_{iz}) = (+1, 0, 0), which represent a sole local directional shearing of voxelated cubes around the x^+ axis, while no shearing around both y and z-axis. Similarly, deformation mode with (n_{ix}, n_{iy}, n_{iz}) = (+1, +1, ±1) in Figure 3d(vii) represents that the column undergoes local shearing around both x^+ and y^+ axis in the middle segment, as well as local shearing around both z^+ and z^- axis in the top and bottom segment.

2.3.3. Combinatorial Multiple Deformation Modes in 3D Metamaterials

To explore the structural response of long-range-order quasi-periodic architecture, based on the polarized spins (n_{ix}, n_{iy}, n_{iz}), we map the ordered quasi-periodic materials onto a directional spin frame (Figure 3e) that satisfies the so-called "ice-rule"[36] (see Section S5.2, Supporting Information for more details). Thus, we can use the simplified "ice-rule" to describe the programmability of our long-range ordered architectures. For example, the different deformation modes of the ith layer consisting of both 2D materials and the (+, +, +) columns shown in Figure 3d can be characterized by the spin configurations with different spin values. We can uniquely correlate each admissible spin configuration to a specific local deformation mode for any allowable structural form of voxelated column. Notably, for the ith layer with (n_{ix}, n_{iy}, n_{iz}) = (±1, ±1, ±1), both 2D materials and the column can deform independently (Figure 3d).

Consequently, the arrangement of spin configurations controls the number of deformation modes of the assembled 3D metamaterials. To this end, we assemble (+,+,+) columns into a three-layered 3D architecture with spin configurations for all layers as (n_{ix}, n_{iy}, n_{iz}) = (±1, ±1, ±1) and fabricate the physical samples by assembling three 6 × 6 units-based 2D material layers connected with two layers of 2 × 3 inserted columns (Figure 3f and Videos S3 and S4, Supporting Information). With the deformation independence between 2D layers and column connectors, the designed 3D metamaterials possess multiple DOFs to achieve unique materials response.

We demonstrate that despite the connections between layers, each layer can deform independently and locally under compression through rigid mode to close the voids without deforming other columns and layers (Mode 1, insets of Figure 3g). It can also be sequentially deformed by laterally compressing the top layer first, followed by column compression through soft mode of cube shearing (Figure 3g). Furthermore, we can achieve globally cooperative deformation modes in the whole structure. For example, $\varepsilon_{xx} = \varepsilon_{yy} = 0$, $\varepsilon_{zz} \neq 0$ (Mode 2, Figure 3h) under vertical compression through local shearing of columns, where ε_{xx}, ε_{yy}, and ε_{zz} denote the macroscopic nominal strains along x, y, and z-axis, respectively. $\varepsilon_{xx} = \varepsilon_{yy} \neq 0$, $\varepsilon_{zz} = 0$ (Mode 3, Figure 3i) under lateral compression through rigid rotation in 2D materials, and $\varepsilon_{xx} = \varepsilon_{yy} \neq 0$, $\varepsilon_{zz} \neq 0$ (Mode 4, Figure 3j) under both vertical and lateral compression through both cooperative column shearing and cube rotation in 2D materials (see Video S4, Supporting Information). Consequently, it results in a 3D auxetic material with a constant negative Poisson's ratio of $\nu_{xy} = \nu_{yx} = -1$ and zero Poisson's ratios of $\nu_{xz} = \nu_{zx} = \nu_{yz} = \nu_{zy} = 0$ in all other planes with $\nu_{ij} = -\varepsilon_{ii} / \varepsilon_{jj}$.

Based on the deformation independence between 2D layers and columns, we could obtain $2^{2N-1} - 1$ ($N \geq 1$) (see Section S5.3, Supporting Information, for more details) disparate combinatory deformation modes for an N-layered 3D metamaterial, providing a potential enormous design space to tune structural forms and programmable material responses. For example, when $N = 10$, it could generate over 5.2×10^5 different deformed configurations (Figure 3k), making this material ultra-programmable. We note that the topological properties of our designed 3D architecture, such as structural anisotropy and deformability, can also be tuned through divergent combinatorial deformation modes of different column types made of distinct cube voxels (Figure S7, Section S6, Video S5, Supporting Information).

2.4. Programmable Deformation Modes

Last, we show that the material response of our proposed 3D architected materials can be manipulated by the multiple deformation modes in the columns under uni-axial compression (Figures S8–S10, Supporting Information, Experimental Section). **Figure 4**a shows the modularly assembled three-layered cardboard prototype composed of 2 × 2 2D lattices (2 × 2 units, green color) bridged by 2 × 2 columns (white color) through the mortise-and-tenon connection method without bonding. The column type chosen here (Figure 4b) has the same hinge arrangements as Figure 3d(i) but with homogeneous cube orientations in the middle segment, resulting in a spin configuration of (n_{ix}, n_{iy}, n_{iz}) = (0, ±1, 0). Interestingly, we find that the cardboard-based columns exhibit excellent elastic recovery after several hundred cycles of loading/unloading tests (Figure S8e, Supporting Information) for their potential reusability.

We note that the architected material demonstrates multimode and nonlinear deformation characterized by the distinct folded structures induced by independent local shearing in the columns (Figure 4b, Video S6, Supporting Information), which lead to four compression modes from Mode 1 to Mode 4 and one interesting shearing mode (Figure 4b,c). For each mode, we conducted the compression tests of the prototype for over 350 times (Figure S8, Section S7, Supporting Information) and calculated stiffness k by the slope of force-compression curves (Figure 4d,e). Overall, we can differentiate the exhibited averaged J-shaped force-compression curves of cardboard samples into two stages (Figure 4d): an initial linear-elastic stage over a long-range attributed to dominated local shearing in the voxelated cubes through hinge-rotation and then transit to a steep strain hardening stage due to cube wall crumpling (see Video S7, Supporting Information). We observe that Mode 1 demonstrates the highest initial stiffness and the stiffness k for the four compression modes is much higher than the shearing mode (Figure 4e), arising from the misaligned deformation of the middle layer. By setting the top column layer with lower torsional hinge stiffness through engraving in the sample (Figure S10, Videos S8 and S9, Supporting Information), we also demonstrate a sequential deformation mode (bottom right of Figure 4c) by deforming the top layer first. Its force-displacement curve in Figure 4f shows four distinct stages accompanied by the monotonic increase of stiffness with the

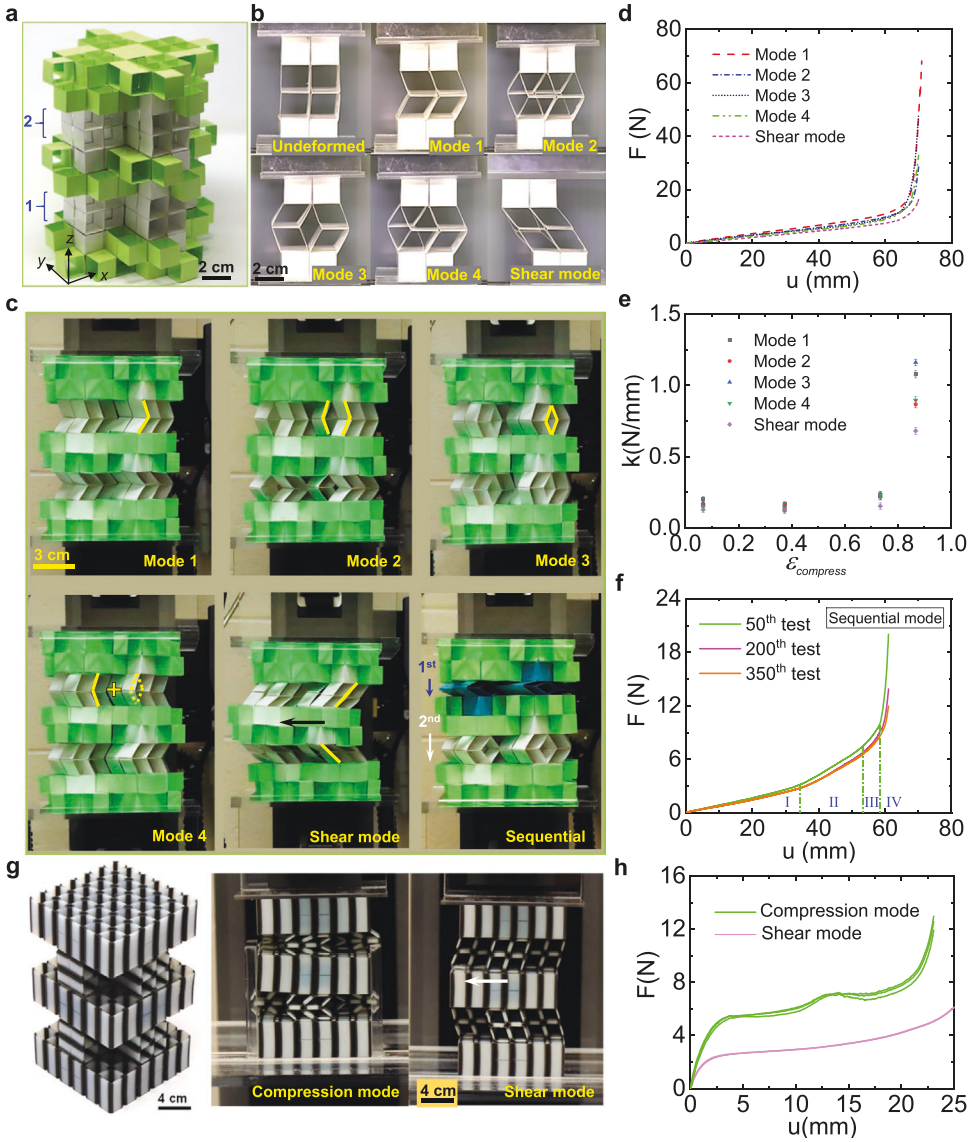

Figure 4. Mechanical properties of 3D metamaterials. a) Prototype of three-layered metamaterials composed of 2 × 2 2D materials and 2 × 2 columns with deformation motif (–, +, –) through modular assembly (see Video S10, Supporting Information, for disassembly process). b) Five deformation modes in the column under compression via cube shearing: four vertical compression modes (Mode 1, 2, 3, and 4) and one shear mode. c) Corresponding five deformation modes in the 3D metamaterials in terms of combinatorial directional shearing in columns and one sequential deformation mode. d–f) Corresponding mechanical properties characterization of the cardboard-based prototype under different deformation modes. (d) Experimental compression force F versus displacement u curves under compression Modes 1–4 and shear mode by averaging 350 compression tests. (e) Corresponding measured structural stiffness under the five deformation modes at four compression strains of 6.7%, 37.3%, 73.3%, and 86.7%. (f) Experimental force-displacement curves under sequential deformation mode at 50th, 200th, and 350th test, showing four-stage deformation and nearly repetitive elastic deformation. g) 3D multi-materials printed prototype (left) and its compression and shear modes (right). Soft hinges are highlighted in black color and hard cube faces are highlighted in white color. h) Experimental force-displacement curves of 3D-printed prototype under shear and compression mode.

compression displacement. Such a sequential deformation mode could provide more tuning space for a programmable multi-step material response for multilayered metamaterials.

3. Discussion

In conclusion, we introduced a 3D modular kirigami approach to design versatile multi-dimensional metamaterials constructed from combinatorial assembly of the same multi-DOF module but in different transformed configurations. The closed-loop connection of the hinged cube module provides a multi-DOF mechanism to transform into versatile daughter modules. Especially, the complimentary transformed configurations between different daughter modules alongside jointless mortise-and-tenon connection method enable assembly, disassembly, and re-assembly into varieties of reusable or new forms of 3D metamaterials (Video S10, Supporting Information)

for materials sustainability and next level of reconfigurability, which could not be achieved in most state-of-art non-disassemblable architected materials.[1–5]

We envision that the proposed design principle and concept is materials and scale-independent, which complies with other materials and fabrication techniques such as additive manufacturing. With the multi-material 3D printing technique (stiff materials for cube walls highlighted in white color and soft rubber-like materials for hinges highlighted in black color, see Figure 4g and Figure S11a, Supporting Information), we demonstrated the applicability and capability of efficiently fabricating our proposed 3D metamaterials through both modular assembly (disassemblable without bonding) and direct printing (non-disassemblable due to bonding between units) without sacrificing programmability and reconfigurability (See more details in Section S8, Supporting Information). The 3D printed metamaterials demonstrate the same programmable and independent deformation modes in the printed column, as well as realize divergent combinatorial structural forms by independently/dependently deforming the column or 2D material layers (Figure 4g,h, Figure S11e,f, Video S11, Supporting Information). Moreover, compared to its cardboard counterpart (Figure 4d), we note that the 3D printed metamaterial exhibits distinct highly nonlinear S-shaped curves with three stages for both compression and shearing deformation modes (Figure 4h), where the shearing mode leads to a more profound stiffness drop. We attribute the different mechanical behavior to the dominated bending in the soft hinges and the rigidity of the non-deformable rigid cube walls, where the soft hinges undergo centroid or off-centroid curve-beam bending during different compression stages. This is different from the coupled bending deformation of both hinges and cubes' thin walls in paper-based samples. Additionally, given the deformations of the unit cell dominated by the thin-plate bending without any micro-twist[37] or compliant rotation mechanism,[38] the mechanical behaviors of our proposed kirigami structure could be adequately captured by the classical linear Cauchy continuum mechanics, and thus would be independent of the unit cell size. Considering their voxelated intrinsic internal structure, we note that the deformation forms and material properties of both paper-based and additively manufactured 3D metamaterials can as well easily be reprogrammed by introducing some pin-like defects[11,12] into columns and/or 2D material layers.

Such a closed-loop connection mechanism could be applied to different numbers of connections and other connected prismatic, tetrahedral, and polyhedron-shaped units or their combination for constructing more varieties of 3D metamaterials with or without bonding connections. In this work, we only explored a small portion of representative structures showing unique materials responses. We believe that the enormous combinations of encoded voxelated cubes with polarized shearing directions and their conformable connections between different modules in each assembled component will largely expand the design space of reconfigurable modular kirigami-inspired metamaterials. The study of these novel materials will provide insight toward the implementation of deformation-controlled, reprogrammable, reusable, and multifunctional materials for minimizing material waste and a range of architectural, phononic, mechanical, and robotic applications.

4. Experimental Section

Fabrication of Single Cardboard Cube with Soft Shearing Mode: The fabrication process of a single cardboard cube is shown in Figure S3, Supporting Information, by following three steps. First, based on the prescribed cutting and engraving patterns for generating respective line cuts and creases in the cardboard, the patterned rectangular strip was cut out with a laser cutter. Second, the non-engraved side of the strip was covered with plastic tape to enhance its reusability and good material elasticity in both the line hinges and thin walls. Third, the strips at the overlapping end were sealed with double-sided tapes and folded the creases by 90° to generate the cardboard cube, see Section S4, Supporting Information, for more details.

Fabrication of 3D Printed Metamaterials: The commercial multiple material 3D printer Stratasys Objet 260 Connex3 was utilized to fabricate the 3D printed architected materials. To realize the hinge rotation mechanism, the line hinges were simplified with printed bendable soft hinges represented by the black curve part (Figure S11a, Supporting Information) with materials of Agilus30Black–FLX 95 550–DM. The thin walls of voxelated cube were printed with stiff materials (RGD 5131–DM). The thickness and length of hinges were 1 and 10 mm with 1 mm inner radius and 2 mm outer radius. The thickness and length of the rigid walls were 1 and 10 mm, respectively (see the schematics in Figure S11a, Supporting Information, and more details in Section S8, Supporting Information).

Mechanical Test: Uniaxial compression tests were conducted for columns with different voxelated cube patterns and 3D architected materials at a rate of 0.01 mms^{-1} (Instron model 5944) to characterize the relation between the compressive force F (N) and the compression displacement u (mm) (see Section S7, Supporting Information, for more details).

Supporting Information

Supporting Information is available from the Wiley Online Library or from the author.

Acknowledgements

The authors thank the help from Dr. Yao Zhao for the scanning electron microscope (SEM) imaging of the cutting samples. The authors acknowledge the funding support from National Science Foundation under award number CMMI-CAREER-2005374.

Conflict of Interest

The authors declare no conflict of interest.

Author Contributions

Y.L. and J.Y. proposed and designed the research. Y.L. designed and fabricated the prototypes. Y.L. performed theoretical analysis of the system. Y.L., Q. Z., and Y.H. performed the experiments. Q.Z. performed the numerical simulation. Y.L. and J.Y. wrote the manuscript. All the authors revised the manuscript.

Data Availability Statement

The data that supports the findings of this study are available in the supplementary material of this article.

Keywords

3D modular kirigami, deformation modes, disassemblable metamaterials, mechanical metamaterials, modular assembly, modular disassembly, programmable properties

Received: June 11, 2021
Revised: July 14, 2021
Published online:

[1] J. Christensen, M. Kadic, O. Kraft, M. Wegener, *MRS Commun.* **2015**, *5*, 453.
[2] A. A. Zadpoor, *Mater. Horiz.* **2016**, *3*, 371.
[3] K. Bertoldi, V. Vitelli, J. Christensen, M. van Hecke, *Nat. Rev. Mater.* **2017**, *2*, 17066.
[4] M. Kadic, G. W. Milton, M. van Hecke, M. Wegener, *Nat. Rev. Phys.* **2019**, *1*, 198.
[5] J. U. Surjadi, L. Gao, H. Du, X. Li, X. Xiong, N. X. Fang, Y. Lu, *Adv. Eng. Mater.* **2019**, *21*, 1800864.
[6] X. Zheng, H. Lee, T. H. Weisgraber, M. Shusteff, J. DeOtte, E. B. Duoss, J. D. Kuntz, M. M. Biener, Q. Ge, J. A. Jackson, S. O. Kucheyev, N. X. Fang, C. M. Spadaccini, *Science* **2014**, *344*, 1373.
[7] R. S. Lakes, *Annu. Rev. Mater. Res.* **2017**, *47*, 63.
[8] O. Sigmund, S. Torquato, *J. Mech. Phys. Solids* **1997**, *45*, 1037.
[9] Q. Wang, J. A. Jackson, Q. Ge, J. B. Hopkins, C. M. Spadaccini, N. X. Fang, *Phys. Rev. Lett.* **2016**, *117*, 175901.
[10] L. Wu, B. Li, J. Zhou, *ACS Appl. Mater. Interfaces* **2016**, *8*, 17721.
[11] Z. G. Nicolaou, A. E. Motter, *Nat. Mater.* **2012**, *11*, 608.
[12] X. Yu, J. Zhou, H. Liang, Z. Jiang, L. Wu, *Prog. Mater. Sci.* **2018**, *94*, 114.
[13] J. N. Grima, K. E. Evans, *J. Mater. Sci. Lett.* **2000**, *19*, 1563.
[14] S. Shan, S. H. Kang, Z. Zhao, L. Fang, K. Bertoldi, *Extreme Mech. Lett.* **2015**, *4*, 96.
[15] J. N. Grima, L. Mizzi, K. M. Azzopardi, R. Gatt, *Adv. Mater.* **2016**, *28*, 385.
[16] Z. Qi, D. K. Campbell, H. S. Park, *Phys. Rev. B* **2014**, *90*, 245437.
[17] Y. Cho, J.-H. Shin, A. Costa, T. A. Kim, V. Kunin, J. Li, S. Y. Lee, S. Yang, H. N. Han, I.-S. Choi, D. J. Srolovitz, *Proc. Natl. Acad. Sci. USA* **2014**, *111*, 17390.
[18] M. K. Blees, A. W. Barnard, P. A. Rose, S. P. Roberts, K. L. McGill, P. Y. Huang, A. R. Ruyack, J. W. Kevek, B. Kobrin, D. A. Muller, P. L. McEuen, *Nature* **2015**, *524*, 204.
[19] Y. Tang, G. Lin, L. Han, S. Qiu, S. Yang, J. Yin, *Adv. Mater.* **2015**, *27*, 7181.
[20] Y. Tang, J. Yin, *Extreme Mech. Lett.* **2017**, *12*, 77.
[21] P. Z. Hanakata, E. D. Cubuk, D. K. Campbell, H. S. Park, *Phys. Rev. Lett.* **2018**, *121*, 255304.
[22] Y.-S. Guan, Z. Zhang, Y. Tang, J. Yin, S. Ren, *Adv. Mater.* **2018**, *30*, 1706390.
[23] Y. Yang, M. A. Dias, D. P. Holmes, *Phys. Rev. Mater.* **2018**, *2*, 110601.
[24] X. Guo, X. Ni, J. Li, H. Zhang, F. Zhang, H. Yu, J. Wu, Y. Bai, H. Lei, Y. Huang, J. A. Rogers, Y. Zhang, *Adv. Mater.* **2021**, *33*, 2004919.
[25] D.-G. Hwang, M. D. Bartlett, *Sci. Rep.* **2018**, *8*, 3378.
[26] N. An, A. G. Domel, J. Zhou, A. Rafsanjani, K. Bertoldi, *Adv. Funct. Mater.* **2020**, *30*, 1906711.
[27] Y. Tang, G. Lin, S. Yang, Y. K. Yi, R. D. Kamien, J. Yin, *Adv. Mater.* **2017**, *29*, 1604262.
[28] R. M. Neville, F. Scarpa, A. Pirrera, *Sci. Rep.* **2016**, *6*, 31067.
[29] N. Yang, J. L. Silverberg, *Proc. Natl. Acad. Sci. USA* **2017**, *114*, 3590.
[30] Y. Tang, Y. Li, Y. Hong, S. Yang, J. Yin, *Proc. Natl. Acad. Sci. USA* **2019**, *116*, 26407.
[31] T. A. Schaedler, W. B. Carter, *Annu. Rev. Mater. Res.* **2016**, *46*, 187.
[32] C. Coulais, E. Teomy, K. de Reus, Y. Shokef, M. van Hecke, *Nature* **2016**, *535*, 529.
[33] J. T. B. Overvelde, T. A. d. Jong, Y. Shevchenko, S. A. Becerra, G. Whiteside, J. C. Weaver, C. Hoberman, K. Bertoldi, *Nat. Commun.* **2016**, *7*, 10929.
[34] X. Fu, D. Guo, X. Liu, G. Pan, Y. Qiao, D. Sun, N. S. Stenhardt, *Chinese Architecture*, Yale University Press, USA **2002**.
[35] D. Shechtman, I. Blech, D. Gratias, J. W. Cahn, *Phys. Rev. Lett.* **1984**, *53*, 1951.
[36] R. F. Wang, C. Nisoli, R. S. Freitas, J. Li, W. McConville, B. J. Cooley, M. S. Lund, N. Samarth, C. Leighton, V. H. Crespi, P. Schiffer, *Nature* **2006**, *439*, 303.
[37] T. Frenzel, M. Kadic, M. Wegener, *Science* **2017**, *358*, 1072.
[38] C. Coulais, C. Kettenis, M. van Hecke, *Nat. Phys.* **2018**, *14*, 40.